

# Large eddy simulation of reactive pollutants in a deep urban street canyon: Coupling dynamics with O<sub>3</sub>-NO<sub>x</sub>-VOC chemistry

Zhong, Jian; Cai, Xiaoming; Bloss, William

DOI:

[10.1016/j.envpol.2017.01.076](https://doi.org/10.1016/j.envpol.2017.01.076)

License:

Creative Commons: Attribution-NonCommercial-NoDerivs (CC BY-NC-ND)

*Document Version*

Peer reviewed version

*Citation for published version (Harvard):*

Zhong, J, Cai, X & Bloss, W 2017, 'Large eddy simulation of reactive pollutants in a deep urban street canyon: Coupling dynamics with O<sub>3</sub>-NO<sub>x</sub>-VOC chemistry', *Environmental Pollution*.  
<https://doi.org/10.1016/j.envpol.2017.01.076>

[Link to publication on Research at Birmingham portal](#)

## **Publisher Rights Statement:**

Eligibility for repository: Checked on 7/3/2017

## **General rights**

Unless a licence is specified above, all rights (including copyright and moral rights) in this document are retained by the authors and/or the copyright holders. The express permission of the copyright holder must be obtained for any use of this material other than for purposes permitted by law.

- Users may freely distribute the URL that is used to identify this publication.
- Users may download and/or print one copy of the publication from the University of Birmingham research portal for the purpose of private study or non-commercial research.
- User may use extracts from the document in line with the concept of 'fair dealing' under the Copyright, Designs and Patents Act 1988 (?)
- Users may not further distribute the material nor use it for the purposes of commercial gain.

Where a licence is displayed above, please note the terms and conditions of the licence govern your use of this document.

When citing, please reference the published version.

## **Take down policy**

While the University of Birmingham exercises care and attention in making items available there are rare occasions when an item has been uploaded in error or has been deemed to be commercially or otherwise sensitive.

If you believe that this is the case for this document, please contact [UBIRA@lists.bham.ac.uk](mailto:UBIRA@lists.bham.ac.uk) providing details and we will remove access to the work immediately and investigate.

# 1 Large eddy simulation of reactive pollutants in a deep urban street 2 canyon: Coupling dynamics with O<sub>3</sub>-NO<sub>x</sub>-VOC chemistry

3 Jian Zhong, Xiao-Ming Cai\* and William James Bloss

4 School of Geography, Earth & Environmental Sciences, University of Birmingham, Edgbaston,  
5 Birmingham, B15 2TT, UK

6 \*Corresponding author. Tel.: (0121) 4145533; Fax: (0121) 4145528.

7 Email address: x.cai@bham.ac.uk (X.-M. Cai).

8

## 9 Abstract:

10 A large eddy simulation (LES) model coupled with O<sub>3</sub>-NO<sub>x</sub>-VOC chemistry is implemented to  
11 simulate the coupling effect of emissions, mixing and chemical pre-processing within an idealised  
12 deep (aspect ratio = 2) urban street canyon under a weak wind condition. Reactive pollutants exhibit  
13 significant spatial variations in the presence of two vertically aligned unsteady vortices formed in  
14 the canyon. Comparison of the LES results from two chemical schemes (simple NO<sub>x</sub>-O<sub>3</sub> chemistry  
15 and a more comprehensive Reduced Chemical Scheme (RCS) chemical mechanism) shows that the  
16 concentrations of NO<sub>2</sub> and O<sub>x</sub> inside the street canyon are enhanced by approximately 30-40% via  
17 OH/HO<sub>2</sub> chemistry. NO, NO<sub>x</sub>, O<sub>3</sub>, OH and HO<sub>2</sub> are chemically consumed, while NO<sub>2</sub> and O<sub>x</sub> (total  
18 oxidant) are chemically produced within the canyon environment. The within-canyon pre-  
19 processing would increase oxidant fluxes released from the canyon to the overlying boundary layer,  
20 and this effect is more crucial for deeper street canyons (as found in many traditional European  
21 urban centres) than shallower (lower aspect ratio) streets. There is clear evidence of distinct  
22 behaviours for emitted chemical species and entrained chemical species, and positive (or negative)  
23 values of intensities of segregations are found between pairs of species with a similar (or opposite)  
24 behaviour. The simplified two-box model underestimated NO and O<sub>3</sub> levels, but overestimated NO<sub>2</sub>  
25 levels for both the lower and upper canyon compared with the more realistic LES-chemistry model.  
26 This suggests that the segregation effect due to incomplete mixing reduces the chemical conversion

27 rate of NO to NO<sub>2</sub>. This study reveals the impacts of nonlinear O<sub>3</sub>-NO<sub>x</sub>-VOC photochemical  
28 processes in the incomplete mixing environment and provides a better understanding of the pre-  
29 processing of emissions within canyons, prior to their release to the urban boundary layer, through  
30 the coupling of street canyon dynamics and chemistry.

31 **Capsule:**

32 The impacts of nonlinear O<sub>3</sub>-NO<sub>x</sub>-VOC photochemical processes in an incomplete mixing  
33 environment are revealed by an LES-chemistry model.

34 **Keywords:**

35 Large eddy simulation; Street canyon; Nonlinear photochemistry; Segregation effect.

36

37

38

39

40

41

42

43

44

45

46

47

## 48    **1 Introduction**

49    Urban air pollution associated with road transport is a major environmental issue (Murena et al.,  
50    2009). Air pollutants in urban areas may be classified into two categories. The first category is  
51    primary air pollutants (Mayer, 1999), which are released directly into the atmosphere from emission  
52    sources (normally resulting from the combustion of fuels) and consist of nitrogen oxides ( $\text{NO}_x$ ) -  
53    primarily NO, volatile organic compounds (VOCs), carbon monoxide (CO) and components of  
54    particulate matter (PM) (Dunmore et al., 2015). The second category is secondary air pollutants,  
55    which are produced into the atmosphere while primary air pollutants undergo chemical reactions  
56    (Jacobson, 2005). As one of the important secondary air pollutants, ozone ( $\text{O}_3$ ) is formed by  
57    chemical reactions involving primarily the oxidation of VOCs and  $\text{NO}_x$  while the sunlight is present.  
58    Fast-reacting chemical radicals (e.g. the hydroxyl radical (OH), and hydroperoxy radical ( $\text{HO}_2$ ))  
59    govern the cycle of the chemical degradation of VOCs ( $\text{O}_3$  precursors) converting NO to  $\text{NO}_2$  and  
60    hence  $\text{O}_3$  formation (Bloss, 2009).

61    The street canyon is normally the basic geometric unit in the built environment of many cities and  
62    typically describes a place with surrounding buildings on both sides of the street (Li et al., 2008b).  
63    Buildings are the artificial obstacles to urban atmospheric flow (Salim et al., 2011) and give rise to  
64    limited ventilation, especially for deep street canyons. The deterioration of urban air quality occurs  
65    due to the combined effects of traffic emissions, dynamics and chemistry within such an  
66    atmospheric compartment (Li et al., 2008b). Investigation of urban air pollution in street canyons  
67    has become a focus of environmental research (Zhong et al., 2016). A variety of approaches, from  
68    full-scale field measurements, reduced-scale physical modelling (e.g. water-channel experiments  
69    and wind-tunnel experiments), numerical modelling (e.g. Computational fluid dynamics (CFD)  
70    models) to parametric (operational) modelling (e.g. street canyon box models), have been  
71    undertaken over recent years to investigate street canyon air quality in urban areas (Vardoulakis et  
72    al., 2003; Ahmad et al., 2005; Li et al., 2006; Yazid et al., 2014). Details of individual aspects of  
73    these approaches can be found in several reviews, e.g. Vardoulakis et al. (2003) focused on full-

74 scale field measurements and parametric (operational) modelling; Ahmad et al. (2005) examined  
75 wind tunnel experiments; Li et al. (2006) used CFD models to understand the dynamical processes  
76 and Yazid et al. (2014) carried out field measurements and modelling studies. Recently, Zhong et al.  
77 (2016) presented a comprehensive review of numerical modelling studies that couple street canyon  
78 dynamics with chemistry of reactive pollutants. Coupling dynamics and chemistry accommodates  
79 the mixing, and photo-chemical processes of emissions. The CFD approach (including mainly  
80 Reynolds-Averaged Navier-Stokes (RANS) and Large-eddy Simulation (LES) models) has become  
81 a powerful tool to investigate high spatial and temporal resolution simulations of wind and pollutant  
82 fields within urban street canyons (e.g. Bright et al., 2013; Kwak et al., 2013; Li et al., 2012).  
83 RANS only provides the information about the mean time-averaged properties, while LES can  
84 predict the additional unsteadiness and intermittency of turbulence (Li et al., 2006). However,  
85 RANS is normally computationally faster than LES (Li et al., 2006).

86 Zhong et al. (2015) employed an LES model to investigate the dispersion and transport of the  
87 reactive species NO, NO<sub>2</sub> and O<sub>3</sub> in a deep urban street canyon by coupling with simple NO<sub>x</sub>-O<sub>3</sub>  
88 chemistry. The turbulent flow derived from the LES model was evaluated against a water-channel  
89 experiment (Li et al., 2008a) and the model agreed well with the experiment in terms of the  
90 velocities, turbulent intensities and flow structure (Zhong et al., 2015). There were spatial  
91 distributions of reactive pollutants driven by the two canyon vortices. A simplified two-box model  
92 coupled with the NO<sub>x</sub>-O<sub>3</sub> chemistry was then developed in the presence of two vortices. This study  
93 further extends the framework used in Zhong et al. (2015), with a focus upon the coupling of the  
94 O<sub>3</sub>-NO<sub>x</sub>-VOC chemistry, rather than simple NO<sub>x</sub>-O<sub>3</sub> chemistry.

## 95 **2 Methodology**

### 96 **2.1 Large-Eddy simulation**

97 The numerical model employed to simulate the incompressible turbulent flow under neutral  
98 conditions in the canyon is based on the LES technique, which computes the larger, grid-resolved

eddy explicitly and parameterises the smaller, unresolved eddies (Liu et al., 2005). The one-equation sub-grid scale (SGS) turbulence model is adopted to model the SGS motions. The near-wall treatment is based on the logarithmic law of the rough-wall model (Schlichting and Gersten, 2000). The LES model is solved by OpenFoam v2.1.1 (OpenFOAM, 2012). The detailed numerical model is described by Zhong et al. (2015).

## 2.2 Coupling with O<sub>3</sub>-NO<sub>x</sub>-VOC chemistry

The filtered governing equations for the transport of reactive pollutants are:

$$\frac{\partial \bar{c}_i}{\partial t} + \frac{\partial}{\partial x_j} (\bar{u}_j \bar{c}_i) = \frac{\partial}{\partial x_j} \left( \left[ \frac{\nu + \nu_{SGS}}{Sc} \right] \cdot \frac{\partial \bar{c}_i}{\partial x_j} \right) + \Delta S_i + E_i \quad (1)$$

Here,  $\bar{c}_i$  is the resolved-scale concentration of the  $i^{th}$  chemical species;  $Sc$  (=0.72) is the Schmidt number (Liu et al., 2005);  $\Delta S_i$  is the chemical source term of the  $i^{th}$  chemical species;  $E_i$  is the emission of the  $i^{th}$  chemical species;  $j$  (=1, 2, 3) denotes the Cartesian component. Due to the computational limitation of LES, a reduced chemical scheme (RCS) with 51 chemical species and 136 chemical reactions (Bright, 2013) is employed as the chemical mechanism in the present study. The RCS was developed and reduced based on the Common Representative Intermediates mechanism version CRI v2-R5 (Jenkin et al., 2008), which included 555 chemical reactions of 196 species. This CRI v2-R5 is a subset of the near-explicit chemical mechanism, i.e. the Master Chemical Mechanism (MCM) (Jenkin et al., 1997) which involves about 13,500 chemical reactions of 5,900 species for MCM v3.1 (Pinho et al., 2007). The MCM has been evaluated against multiple chamber and field datasets (Bloss et al., 2005; Saunders et al., 2003; Jenkin et al., 1997; Jenkin et al., 2003) and can be a benchmark mechanism for the development and evaluation of reduced chemical mechanisms. Both the RCS and CRI have been evaluated regarding the abundance of key oxidants for the daytime scenarios compared to the MCM (Bright, 2013; Bright et al., 2013). The largest difference of OH between the RCS (reduced from CRI) and MCM was about 6% over a four

hour box model simulation (Bright, 2013; Bright et al., 2013), which was acceptable compared with the errors associated with the OH measurement of 7-16 % (Heard and Pilling, 2003).

A challenge to solve the transport equations for reactive pollutants (especially fast-reacting chemical radicals, e.g. OH and HO<sub>2</sub>) is to derive the chemical source terms. According to Hertel et al. (1993), the ordinary differential equations of a chemical system can be described as follows:

$$\frac{dc_i}{dt} = P_i - L_i c_i \quad i = 1, 2, \dots, nc \quad (2)$$

Here,  $nc$  is the total number of the chemical species,  $i$  represents the  $i^{th}$  chemical species,  $c_i$  is the concentration,  $P_i$  is the chemical production term and  $L_i$  is the chemical loss rate ( $L_i c_i$  therefore represents the chemical loss term). Both  $P_i$  and  $L_i$  are non-negative functions of concentrations, i.e.

$$P_i = P_i(t, c_1, c_2, \dots, c_{nc}) \quad (3)$$

$$L_i = L_i(t, c_1, c_2, \dots, c_{nc}) \quad (4)$$

The chemical timescale of the  $i^{th}$  chemical species  $\tau_i$  (Neophytou et al., 2004) is defined as follows:

$$\tau_i = \frac{1}{L_i} \quad (5)$$

The chemical system is normally stiff due to the variability (from very fast to rather slow) of the chemical time scale (Verwer and Simpson, 1995). The QSSA (quasi-steady-state approximation) algorithm has been widely used to handle stiff chemical systems in air pollution modelling (e.g. Hesstvedt et al., 1978; Verwer and Vanloon, 1994). The QSSA algorithm is described below.

$c_i^n$  denotes the concentration of the  $i^{th}$  chemical species at  $t = t_n$ . It is assumed that  $P_i$  and  $L_i$  in Equation (2) are constant over a given time step  $\Delta t$  (Hertel et al, 1993),

$$t_{n+1} = t_n + \Delta t \quad (6)$$

Equation (2) may be solved analytically by the following formula:

$$c_i^{n+1} = \frac{P_i^n}{L_i^n} + (c_i^n - \frac{P_i^n}{L_i^n})e^{-L_i^n \Delta t} \quad (7)$$

Depending on the chemical timescales and time steps, three categories of formulae are derived (Alexandrov et al., 1997). (i) If  $\tau_i < \frac{\Delta t}{10}$ , it means that the chemical reaction is very fast over the given time step. The steady state at the end of the time step can be assumed and Equation (7) can be expressed by the following approximation,

$$c_i^{n+1} = \frac{P_i^n}{L_i^n} \quad (8)$$

(ii) If  $\Delta t / 10 \leq \tau_i \leq 100\Delta t$ , it means that the chemical reaction is at a medium rate over the given time step and Equation (7) is applied. (iii) If  $\tau_i > 100\Delta t$ , it means that the chemical reaction is rather slow over the given time step and the forward Eulerian formula can be employed,

$$c_i^{n+1} = c_i^n + (P_i^n - L_i^n c_i^n)\Delta t \quad (9)$$

The QSSA algorithm has simple formulae and can be easily employed in large air pollution models. However, there are also some drawbacks. At each cell for each species, there are three formulae to be conditionally determined. It demands more computational time for the air pollution models with a huge number of cells. In addition, the computational cost to compute the exponential function in Equation (7) is expensive. Therefore, an attempt has been conducted (Alexandrov et al., 1997) to improve the performance of the QSSA algorithm. The exponential function can be rationally approximated by the following expression based on the Taylor expansion in the second order:

$$e^{-L_i^n \Delta t} \approx \frac{1}{1 + L_i^n \Delta t + 0.5(L_i^n \Delta t)^2} \quad (10)$$

Then Equation (7) can be rewritten as:



$$c_i^{n+1} = \frac{c_i^n + (1 + 0.5L_i^n \Delta t)P_i^n \Delta t}{1 + L_i^n \Delta t + 0.5(L_i^n \Delta t)^2} \quad (11)$$

In this study, the chemical species in the RCS chemical mechanism can be separated into two groups, i.e. slower chemical species (e.g. NO<sub>x</sub> and O<sub>3</sub>) and faster chemical species (e.g. OH and HO<sub>2</sub>). For slow chemical species, a time step of 0.03 s (Bright et al., 2013) is adopted and Equation (9) is used. For fast chemical species, the above-mentioned QSSA algorithm with Equation (11) (with a smaller time step of 0.003 s) (Bright et al., 2013) is adopted.

### 2.3 Model setup

The computational domain in the study is same as that in Zhong et al. (2015), shown as Figure S1 (in the Supplementary Materials), which consists of an idealised deep street canyon (AR=2, i.e.  $H=36$  m and  $W=18$  m). A constant pressure gradient above the canyon (perpendicular to the street axis) is used to drive the street canyon flow. Symmetry boundary conditions are used at the domain top for both the flow and pollutants. Cyclic boundary conditions are used in both the  $x$ - and  $y$ -directions for the flow. For pollutants, the inlet adopts “fixed-value” boundary conditions. A photochemical box model (including the RCS mechanism) is run without emissions for 30 mins in order to achieve a photochemical pseudo-equilibrium condition. Then concentrations of all chemical species at  $t=30$  min are used as their inlet boundary conditions. For the outlet, the advective boundary condition

$$\frac{\partial \bar{c}_i}{\partial t} + \bar{u} \frac{\partial \bar{c}_i}{\partial x} = 0 \quad (12)$$

is employed. On the solid boundaries, the near-wall treatment (Schlichting and Gersten, 2000) is employed for the flow and zero-gradient conditions are used for pollutants (assuming no pollutant deposition). At  $t=30$  min, the chemistry mechanism and emissions modules are switched on in the presence of canyon dynamics, i.e. a statistically steady turbulent flow derived from the LES model (Zhong et al., 2015), for a 210 min duration window ( $t=30$  to 240 min).

185 Emissions are represented by two traffic lanes with a Gaussian distribution located at  $z = 1$  m and at  
 186 2.5 m from both sides of the street centre (Zhong et al., 2015). Based on the UK Road Vehicle  
 187 Emission Factors (Boulter et al., 2009), emission rates for  $\text{NO}_x$ , VOCs and CO of 620, 128 and  
 188  $1,356 \text{ g km}^{-1} \text{ hr}^{-1}$  (equivalent to  $1,000 \text{ ppb s}^{-1}$ ,  $3,593 \text{ ppb s}^{-1}$ , and  $691 \text{ ppb s}^{-1}$  respectively released  
 189 into a typical LES model cell, i.e.  $0.3 \text{ m} \times 1 \text{ m} \times 0.3 \text{ m}$  in the  $x$ -,  $y$ - and  $z$ -directions) were used.  
 190 This emission scenario approximately represents urban continuous road traffic of  $1,500 \text{ vehicles hr}^{-1}$   
 191 with an average speed of 30 mph (Boulter et al., 2009). The fractional  $\text{NO}_x$  emission rate by volume  
 192 is 90% for NO and 10% for  $\text{NO}_2$  (Baker et al., 2004). The fractional VOCs emission rate by volume  
 193 is 44% for ethane ( $\text{C}_2\text{H}_4$ ), 19% for propene ( $\text{C}_3\text{H}_6$ ), 25% for formaldehyde ( $\text{HCHO}$ ) and 12% for  
 194 acetaldehyde ( $\text{CH}_3\text{CHO}$ ) (Bright et al., 2013).

195 Computation of the LES model coupling the RCS mechanism (LES-chemistry) was performed in  
 196 the University of Birmingham's Linux-based High Performance Computing (HPC) cluster. In this  
 197 research, the total number of cores used was 32, i.e. the LES-chemistry model was run in parallel on  
 198 2 nodes, each of which consists of 16 cores with 64-bit 2.2 GHz processors and 32 GB of memory.  
 199 The total computation time for the LES-chemistry was about 10 days.

### 200 **3 Post-processing of LES output**

201 The 3-D fields (at each grid) for wind and concentrations were stored in interval time step of 3s and  
 202 the final hour of the simulation ( $t = 180$  to  $240$  min) was used to analyse the resolved-scale  
 203 turbulent statistics. The temporal average over  $t \in [t_1, t_2]$  and spatial average over  $y \in [0, L_y]$  of any  
 204 resolved-scale quantity  $\bar{\phi}$  gives a 2D function  $\langle \bar{\phi} \rangle(x, z)$ , i.e.

$$205 \quad \langle \bar{\phi} \rangle(x, z) = \frac{1}{L_y(t_2 - t_1)} \int_{t_1}^{t_2} \int_0^{L_y} \bar{\phi}(x, y, z, t) dy dt \quad (13)$$

206 and  $\phi'(x, y, z, t) = \bar{\phi}(x, y, z, t) - \langle \bar{\phi} \rangle(x, z)$  denotes the resolved-scale fluctuation component of  $\bar{\phi}$   
 207 about  $\langle \bar{\phi} \rangle$ .

### 208 **3.1 Decomposition of contributions from emission and chemistry**

209 For a passive scalar (i.e. a non-reactive scalar), abundance within a street canyon is determined by  
 210 the emission rate and the background concentration of the passive scalar once the street canyon  
 211 turbulent flow is given. We denote its  $t$ - and  $y$ -averaged spatial field as  $\langle \bar{C}_{ps} \rangle$ . For a reactive scalar  
 212 (e.g. NO<sub>2</sub>), in addition to the contribution from its emission rate and background concentration, the  
 213 contribution from chemistry also affects its abundance within the street canyon. If the mean  
 214 concentration for any chemical species inside an idealised 2D street canyon derived from LES is  
 215 denoted by  $\langle \bar{C} \rangle(x, z)$ , we can then define the contribution to its abundance from chemistry, denoted  
 216 by  $\langle \bar{C}_{chem} \rangle$ , using the following equation (without loss of generality, the overbar and the angle  
 217 brackets of all terms are dropped for the purpose of presentation):

$$218 \quad C_{chem}(x, z) = C(x, z) - C_{ps}(x, z) \quad (14)$$

219 Further,

$$220 \quad C_{ps}(x, z) = C_b(x, z) + C_{emn}(x, z) \quad (15)$$

221 Here, ‘b’ is for ‘background’ and ‘emn’ is for ‘emission’.  $C_{emn}(x, z)$  is the field of the passive scalar  
 222 induced by the given emission and corresponding to ‘zero background’.  $C_b(x, z)$  is the spatial  
 223 distribution induced by an upwind background concentration of  $C_0$ . It is assumed that

$$224 \quad C_b(x, z) = C_0 = const \quad (16)$$

225 This assumption is true if the system is allowed to achieve a steady state; air inside the canyon will  
 226 be in balance with the above-roof concentration and should be constant. Thus,

$$C_{ps}(x, z) = C_0 + C_{em}(x, z) \quad (17)$$

It is assumed that  $C_{em}(x, z)$  linearly scales with the emission rate. It is further defined that  $C_{em,1}(x, z)$  is the concentration for a unit emission rate and  $C_{em,1}(x, z)$  can be derived from the LES simulation for a passive scalar (with zero background). Therefore,

$$C_{em}(x, z) = E * C_{em,1}(x, z) \quad (18)$$

where  $E$  is the emission rate for this species. In such a way, a spatial pattern of a passive scalar can be used to reconstruct the pattern for any other passive scalars, or the emission-induced component of a non-passive scalar.

Therefore, the contribution from chemistry to any non-passive scalar can be diagnosed by following equation:

$$C_{chem}(x, z) = C(x, z) - E * C_{em,1}(x, z) - C_0 \quad (19)$$

in which both  $C(x, z)$  and  $C_{em,1}(x, z)$  are derived from LES with prescribed  $E$  and  $C_0$ . This formula can be applied for all emitted species (e.g. NO, NO<sub>2</sub>, NO<sub>x</sub> and O<sub>x</sub>). In particular, for any non-emitted species (e.g. O<sub>3</sub>, OH and HO<sub>2</sub>), the contribution from emission is effectively ignored and therefore the contribution from chemistry is simply obtained:

$$C_{chem}(x, z) = C(x, z) - C_0 \quad (20)$$

A negative (positive) value of  $C_{chem}$  means the chemical consumption (production). A zero value of  $C_{chem}$  means no chemical consumption or production. For higher-order reactions,  $C_{chem}$  is also a function of the background concentrations and the emission rates of relevant chemical species. This complexity due to the nonlinearity of the chemical processes, however, does not limit the

247 application of such analysis for the purpose of diagnosis under a given set of conditions (i.e.  
248 background concentrations and emission rates).

249 The Damköhler number (Da), defined as the ratio of the turbulent mixing timescale ( $T_{\text{mix}}$ ) to the  
250 chemical timescale ( $T_{\text{chem}}$ ), can be used to investigate the combined effect between dynamics and  
251 chemistry (Auger and Legras, 2007). When  $\text{Da} \ll 1$ , chemical processes are rather slow compared  
252 with dynamical processes and chemical species may be regarded as well-mixed scalars with  
253 minimal segregation effects. When  $\text{Da} \gg 1$ , chemistry is very fast and can achieve a chemical  
254 equilibrium before the flow mixes together chemical species. In such situations, the interaction  
255 between dynamics and chemistry is very important with substantial segregation effects.

### 256 **3.2 Vertical advective and turbulent fluxes of pollutants**

257 The vertical advective flux of any species at the resolved-scale is defined:

$$258 \quad F_{\text{adv}}(x, z) = \langle \bar{w} \rangle(x, z) \langle \bar{\phi} \rangle(x, z) \quad (21)$$

259 and the vertical turbulent flux is defined:

$$260 \quad F_{\text{turb}}(x, z) = \langle w' \phi' \rangle(x, z) = \frac{1}{L_y(t_2 - t_1)} \int_{t_1}^{t_2} \int_0^{L_y} w'(x, y, z, t) \phi'(x, y, z, t) dy dt \quad (22)$$

261 Thus the vertical total flux is obtained as follows:

$$262 \quad F_{\text{total}}(x, z) = F_{\text{turb}}(x, z) + F_{\text{adv}}(x, z) \quad (23)$$

263 These quantities of fluxes represent the 2D spatial variation. For the purpose of discussion, these  
264 quantities are further averaged horizontally and vertical profiles are derived:

$$265 \quad F(z) = \frac{1}{W} \int_{-0.5W}^{0.5W} F(x, z) dx \quad (24)$$

### 266 3.3 Intensity of segregation

267 In order to characterise the segregation effect due to incomplete mixing of chemical species, a  
 268 widely used dimensionless number, the *intensity of segregation* (Krol et al., 2000) between two  
 269 chemical species A and B,  $I_{S(A+B)}$ , is introduced and defined as:

$$270 \quad I_{S(A+B)} = \frac{1}{W * H} \int_{-0.5W}^{0.5W} \int_0^H \frac{A'(x,z) * B'(x,z)}{[A] * [B]} dx dz \quad (25)$$

271 where  $[A]$  and  $[B]$  represent the canyon averages of  $\langle \bar{A} \rangle(x,z)$  and  $\langle \bar{B} \rangle(x,z)$ , respectively, in which  
 272  $\langle \bar{A} \rangle(x,z)$  and  $\langle \bar{B} \rangle(x,z)$  are derived from Equation (13); the prime  $A'(x,z) = \langle \bar{A} \rangle(x,z) - [A]$  (or  
 273  $B'(x,z) = \langle \bar{B} \rangle(x,z) - [B]$ ) denotes the local spatial deviation from the canyon-averaged  
 274 concentration, and  $A'(x,z) * B'(x,z)$  stands for the spatial covariance between A and B. The  
 275 intensity of segregation is a proper measure of the effect of spatial segregation on nonlinear  
 276 chemical processes (Hilst, 1998) and represents the deviation from a well-mixed environment due  
 277 to the coupling between dynamics and chemistry (Zhong et al., 2014). For a second-order reaction  
 278  $A+B \rightarrow C$  in a heterogeneous system, the rate of formation of C (Vinuesa and de Arellano, 2005)  
 279 evaluated for the *whole* volume of air *inside* the street canyon in the framework of one-box model  
 280 can be described as follows,

$$281 \quad \frac{d[C]}{dt} = k_{eff(A+B)} [A][B] \quad (26)$$

282 where  $k_{eff(A+B)}$  is the effective second-order rate constant for formation of C in the heterogeneous  
 283 system, i.e.

$$284 \quad k_{eff(A+B)} = k_{(A+B)} (1 + I_{S(A+B)}) \quad (27)$$

285 where  $k_{(A+B)}$  is the original rate constant of the reaction in a well-mixed system. Such a constant is  
286 normally obtained from laboratory experiments in a well-mixed chamber. If  $I_{S(A+B)} = 0$ , it means  
287 that species A and B can be regarded as well-mixed; If  $I_{S(A+B)} > 0$  or  $I_{S(A+B)} < 0$ , it implies that  
288  $k_{eff(A+B)}$  in the heterogeneous system is larger or smaller than  $k_{(A+B)}$  in the well-mixed system due to  
289 the effect of segregation. Segregation effect for the street canyon environment will be investigated  
290 in this study.

## 291 4 Results and discussion

### 292 4.1 Spatial variation of reactive pollutants

#### 293 4.1.1 Spatially and temporally averaged concentrations

294 Figure 1 illustrates the spatial variation of (a)  $\langle \overline{NO} \rangle$ , (b)  $\langle \overline{NO_2} \rangle$ , (c)  $\langle \overline{O_3} \rangle$ , (d)  $\langle \overline{NO_x} \rangle$ , (e)  $\langle \overline{O_x} \rangle$ , (f)  
295  $\langle \overline{NO} \rangle / \langle \overline{NO_2} \rangle$ , (g)  $\langle \overline{OH} \rangle$  and (h)  $\langle \overline{HO_2} \rangle$  (See Equation (13); averaged from 180 to 240 min).  
296 These plots show the influence of two primary vortices on pollutant dispersion as observed by  
297 Zhong et al. (2015) with simple  $NO_x$ - $O_3$  chemistry. Figure 1a-c show similar spatial patterns of NO,  
298  $NO_2$  and  $O_3$  as those in Zhong et al. (2015) (Figure 4a-c in their study). There are sinks of  $NO_x$  and  
299 sources of  $O_x$  in the current study (with the  $O_3$ - $NO_x$ -VOC chemistry). However,  $NO_x$  and  $O_x$  are  
300 effectively conserved in Zhong et al. (2015) (with simple  $NO_x$ - $O_3$  chemistry).  $NO_x$  plays a key role  
301 in the street-canyon atmospheric chemistry.  $NO_2$  levels are largely determined by the within-canyon  
302 processing through the chemical reactions of NO with other species (e.g.  $O_3$  titration and also  
303 OH/ $HO_2$  chemistry). Both  $NO_x$  and  $O_x$  are useful measures of the street-canyon atmospheric  
304 chemistry (Figure 1d-e). The ratio of NO/ $NO_2$  (Figure 1f) is a useful indicator of chemical  
305 interactions within the street canyon, reflecting the conversion of NO to  $NO_2$  through chemistry.  
306 The NO/ $NO_2$  ratio also had a similar pattern driven by two vortices, ranging from about 3.6 (vs 6 in  
307 Zhong et al., 2015) at the right of lower canyon to about 1.4 (vs 3 in Zhong et al., 2015) at the

canyon roof level. The NO/NO<sub>2</sub> ratio within the street canyon was much lower compared to the raw emission ratio of NO/NO<sub>2</sub> (assumed as a value of 9). This reflected the contributions of directly emitted NO<sub>2</sub> and chemical oxidation of emitted NO to increased levels of NO<sub>2</sub>. The fast reacting chemical radicals (OH and HO<sub>2</sub>) played a key role in the additional conversion of NO to NO<sub>2</sub> through OH/HO<sub>2</sub> chemistry. The spatial distributions of OH and HO<sub>2</sub> (Figure 1g-h) had similar patterns to that of O<sub>3</sub>, in which their background mixing ratios were much higher than those within the canyon (averagely by a factor of about 2 for OH, 5 for HO<sub>2</sub> and 3 for O<sub>3</sub>).

#### 4.1.2 Simple NO<sub>x</sub>-O<sub>3</sub> chemistry vs O<sub>3</sub>-NO<sub>x</sub>-VOC chemistry

Figure 2 illustrates spatial variations of the overestimation of the spatially and temporally averaged concentrations (%) by simple NO<sub>x</sub>-O<sub>3</sub> chemistry (Zhong et al., 2015) compared with the RCS mechanism (O<sub>3</sub>-NO<sub>x</sub>-VOC chemistry) in this study for (a)  $\langle \overline{NO} \rangle$ , (b)  $\langle \overline{NO_2} \rangle$ , (c)  $\langle \overline{O_3} \rangle$ , (d)  $\langle \overline{NO_x} \rangle$ , (e)  $\langle \overline{O_x} \rangle$  and (f)  $\langle \overline{NO} \rangle / \langle \overline{NO_2} \rangle$ . Generally, simple NO<sub>x</sub>-O<sub>3</sub> chemistry overestimates the levels of NO, NO<sub>x</sub> and NO/NO<sub>2</sub>, but underestimates the levels of NO<sub>2</sub>, O<sub>3</sub> and O<sub>x</sub>. Such findings suggest that using simple NO<sub>x</sub>-O<sub>3</sub> chemistry may provide a reasonable prediction of air pollution in street canyon (for NO<sub>2</sub> - i.e. predicted levels are biased low) while in reality the NO<sub>2</sub> level may exceed the air quality standards, which may mislead a policy-maker to make an inappropriate decision with respect to air quality management. There are some common features for these overestimations (biases) in Figure 2. At the canyon roof level, a sharp decrease of the magnitudes of those biases was observed and those values approach to zero for the wider background. The largest values of the magnitudes of overestimation (about 30 % for NO, about -38% for NO<sub>2</sub>, about -52% for O<sub>3</sub>, about 4% for NO<sub>x</sub>, about -40% for O<sub>x</sub> and about 115% for NO/NO<sub>2</sub>) were found close to the centre of the upper vortex. For air pollution problems related to higher levels of NO<sub>2</sub> in urban areas, an underestimation of NO<sub>2</sub> by 40% could be a substantial issue (Defra, 2008). In the lower part of the canyon, the magnitudes of those overestimations were comparatively low and generally decrease down to the street ground - this is of significance as the region in which receptor / population exposure occurs (at heights of 1 - 2 m). It is noted that there was a slight overestimation for NO<sub>x</sub> by the simple chemistry and this was



334 due to the extra sink of  $\text{NO}_x$  to other N-contained species (such as Nitric acid ( $\text{HNO}_3$ ) and Nitrous  
335 acid ( $\text{HONO}$ )) presented in the more comprehensive RCS. It is interesting that there is a large  
336 underestimation for the oxidants ( $\text{NO}_2$ ,  $\text{O}_3$  and  $\text{O}_x$ ) by the simple chemistry. This is attributed to the  
337 additional conversion of  $\text{NO}$  to  $\text{NO}_2$  by the  $\text{OH}/\text{HO}_2$  chemistry in the RCS, exacerbated by limited  
338 exchange in this deep canyon scenario.

#### 339 4.1.3 Vertical profiles of concentrations

340 Figure 3 depicts vertical profiles of (a)  $\langle \overline{\text{NO}} \rangle$ , (b)  $\langle \overline{\text{NO}_2} \rangle$ , (c)  $\langle \overline{\text{NO}_x} \rangle$ , (d)  $\langle \overline{\text{O}_x} \rangle$ , (e)  $\langle \overline{\text{NO}} \rangle / \langle \overline{\text{NO}_2} \rangle$ ,  
341 (f)  $\langle \overline{C} \rangle / C_b$  along the leeward and windward buildings, respectively. For the upper (or lower) vortex,  
342  $\text{NO}$ ,  $\text{NO}_2$ ,  $\text{NO}_x$ ,  $\text{O}_x$  and  $\text{NO}/\text{NO}_2$  at the vicinity of the leeward building were generally higher (lower)  
343 than those of the windward building (Figure 3a-e). But for  $\text{O}_3$ , the situation is reversed (Figure 3f).  
344 For the  $\text{AR}=1$  case, there are higher concentrations of emitted pollutants towards the leeward  
345 building at the pedestrian level (e.g. Baker et al., 2004; Kwak and Baik, 2012). However, for the  
346  $\text{AR}=2$  case, higher concentrations of emitted pollutants (e.g.  $\text{NO}_x$ ) are observed towards the  
347 windward building at the pedestrian level (due to the opposite direction between the upper vortex  
348 and lower vortex) (Figure 3a-e). It was also interesting to note that just above the canyon roof level  
349 ( $z/W=2$ ), there were much higher levels of pollutants (e.g.  $\text{NO}_x$ ) at the windward side (i.e. the  
350 canyon outlet) than those at the leeward side (i.e. the canyon inlet) (Figure 3a-e). This reflected  
351 increased levels of pollutants transferred from the canyon to the wider ambient environment, which  
352 highlighted the importance of the coupling effect of emissions, mixing and chemical pre-processing  
353 within the street canyon. The windward side was the main location of this street canyon ventilation  
354 system, potentially taking ambient air into buildings. The vertical profiles of  $\text{OH}$  and  $\text{HO}_2$  have  
355 similar patterns to that of  $\text{O}_3$ , in which their levels along both the leeward and windward walls  
356 increased with the vertical height and approach to their corresponding background concentrations at  
357 approximately  $z/W=2.4$ . In the upper (or lower) part of the canyon, the mixing ratios of  $\text{OH}$  and  
358  $\text{HO}_2$  along the windward wall were slightly higher (or lower) than those along the leeward wall. For

comparison, levels of  $O_3$ , OH and  $HO_2$  are normalised by their background concentrations (Figure 3f). It was observed that  $HO_2$  had the sharpest drop near the canyon roof level while  $O_3$  decreased the least. This suggested that either  $HO_2$  or OH is more rapidly consumed (sharp shift) than  $O_3$  at the canyon roof level as the above canyon air is entrained into the canyon. Within the canyon, there was a similar consumption rate for OH and  $HO_2$ , but much slower than that for  $O_3$ . The rapid  $O_3$  consumption inside the canyon can be explained by  $NO_x$  (NO) emissions from the street level, which had a strong titration effect thereby leading to the rapid consumption of  $O_3$ .

#### 4.1.4 Contributions from emission and chemistry

Figure 4 illustrates the spatial variations of (a)  $C_{em,1}$  and  $C_{chem}$  of (b) NO, (c)  $NO_2$ , (d)  $NO_x$ , (e)  $O_x$ , (f)  $O_3$ , (g) OH and (h)  $HO_2$  (See Equations (18), (19) and (20)). The spatial pattern of a passive scalar with a unit emission rate is depicted in Figure 4a. It was observed that the distribution of the passive scalar can be characterised by the two unsteady vortices formed inside the street canyon (Cross-sectional flow structure can be seen from Fig. 3 of the LES simulation in Zhong et al. 2015). The emission of the passive scalar was mainly trapped inside the lower vortex closer to the windward wall. This unit emission rate scenario was used to reconstruct the spatial pattern based on Equation (19) for the chemistry-induced component of a non-passive scalar in Figure 4 b-e. It was found that NO,  $NO_x$ ,  $O_3$ , OH and  $HO_2$  were chemically consumed (negative values of  $C_{chem}$ ). For  $NO_2$  and  $O_x$ , however, chemical production occurred inside the street canyon (positive values of  $C_{chem}$ ). The chemical consumption of NO and  $O_3$  was largely caused by the titration effect and by the (slow, but important near emission source)  $NO + NO + O_2$  reaction. The concentration contributed from the chemical consumption for  $NO_x$  was about 14% of that for NO. The slight chemical consumption of  $NO_x$  indicated that there was a sink of  $NO_x$  in the chemical processing, but this rate was relatively slow on the canyon timescale. The concentration contributed to the chemical production for  $O_x$  was about 67% of that for  $NO_2$ . This was partially attributed to the chemical consumption of  $O_3$  in the canyon. The chemical production of  $O_x$  was due to VOC

oxidation processes through the chemistry associated with fast radicals (e.g.  $\text{HO}_x$ ) which effectively convert NO to  $\text{NO}_2$ . It was observed that  $C_{chem}$  for OH and  $\text{HO}_2$  were negative, i.e. chemically consumed in the street canyon environment. The spatial patterns for these  $C_{chem}$  were dependent upon the vortex structure inside the street canyon. There were also sharp gradients at the canyon roof level and a clear separation at the interface between the lower and upper vortices. It is interesting to note that the greatest magnitudes of either positive or negative values were observed close to the windward wall in the lower vortex. These may be explained by the trapped emissions due to the anti-clockwise vortex in the lower canyon and the relatively longer retention time than that in a much shallower canyon with an  $\text{AR}=1$ . These magnitudes for the upper canyon were slightly lower than those for the lower canyon. It was also noted that in the background atmosphere above the canyon, there was no chemical production or consumption (the values of  $C_{chem}$  being close to zero). This was due to that the background atmosphere was already in the quasi-equilibrium state, in the simulation approach adopted here (although not necessarily in reality, with upwind heterogeneity). The turbulent mixing timescale ( $T_{mix}$ ) can be estimated as the length scale of the canyon divided by its velocity scale. The length scale of the canyon is  $H$  ( $=36$  m) and the velocity scale of turbulent mixing is estimated as  $0.058 \text{ m s}^{-1}$ , i.e. the square root of the mean resolved-scale turbulent kinetic energy (Salizzoni et al., 2009). The turbulent mixing timescale was calculated as 621 s. The chemical timescales ( $T_{chem}$ ) within the canyon (calculated based on Equation (5) using the canyon averaged quantities over the last 60 min period) was estimated as 185 s for NO, 108 s for  $\text{NO}_2$ , 9 s for  $\text{O}_3$ , 0.0043 s for OH and 0.014 s for  $\text{HO}_2$ . The Damköhler number (Da) was calculated as 3.4 for NO, 5.8 for  $\text{NO}_2$ , 69 for  $\text{O}_3$ ,  $1.44 \times 10^5$  for OH, and  $4.44 \times 10^4$  for  $\text{HO}_2$ . This reflected that the chemical production or consumption for these species was limited by dynamical processes in the street canyon environment (Figure 4 b-h). In other words, the local chemistry dominated the relative abundance of  $\text{HO}_x$  and probably  $\text{O}_3$  ( $\text{Da} \gg 1$ ), but for NO and  $\text{NO}_2$ , the interaction between dynamics and chemistry was of vital importance (the turbulent mixing timescale was comparable to the chemical timescale, as Da was in the same order as 1).

## 410    **4.2 Pre-processing of emitted pollutants**

411    Figure 5 shows vertical profiles of the horizontally averaged total (Equation 23), turbulent  
412    (Equation 22) and advective (Equation 21) fluxes, for (a) NO, (b) NO<sub>2</sub>, (c) O<sub>3</sub>, (d) NO<sub>x</sub>, (e) O<sub>x</sub> and  
413    (f) NO/NO<sub>2</sub>. The relative total fluxes for non-passive scalars were reconstructed based on a passive  
414    scalar with a unit emission rate (Figure 4a) and were denoted by the red solid lines. The departure  
415    of the total fluxes (black solid lines) away from the red solid lines represents chemically induced  
416    fluxes. Negative (or positive) values of fluxes mean that pollutants are entrained downward (or  
417    upward) to the street canyon. It was observed that advective fluxes were higher than turbulent  
418    fluxes for both upper and lower vortices, but lower for shear layers, which indicated that advective  
419    fluxes acted as a dominant mechanism for the transport of pollutant within a vortex while turbulent  
420    fluxes played an important role for the exchange of pollutants within the zone between the vortices.  
421    There was also clear evidence that both advective fluxes and turbulent fluxes change rapidly close  
422    to the canyon roof level and the level where two vortices formed in the deep street canyon  
423    interacted. This sensitivity to the vertical height at the canyon roof level was also found by Cheng  
424    and Liu (2011a), in which LES simulations of a passive scalar in the street canyon with AR=1 were  
425    conducted. A positive (upward) total flux was observed for emitted species (e.g. NO and NO<sub>2</sub>)  
426    while a negative (downward) total flux was observed for entrained species (e.g. O<sub>3</sub>). Total fluxes for  
427    emitted species (e.g. NO and NO<sub>2</sub>) increased rapidly from the ground to the level at  $z/W=0.1$   
428    (where the centre of the elevated emissions is located), and then decreased with height in the  
429    canyon for NO, but increased with height for NO<sub>2</sub>. This reflects the chemical conversion of NO to  
430    NO<sub>2</sub> through within-canyon pre-processing of emissions. The NO/NO<sub>2</sub> ratio of total fluxes was  
431    about 1.7 (vs 4 in Zhong et al., 2015) at the canyon roof level, smaller than the NO/NO<sub>2</sub> ratio of the  
432    emission fluxes (assumed as 9:1). Therefore, the within-canyon processing resulted in increased  
433    levels of NO<sub>2</sub> through the chemical conversion of NO to NO<sub>2</sub> and changed the partitioning of total  
434    NO<sub>x</sub> emissions at the canyon roof level. This indicated that apart from the emitted NO<sub>2</sub>, the  
435    chemical processing within the canyon had a substantial contribution to the high level of NO<sub>2</sub>

436 released to the overlying canopy layer. For  $\text{NO}_x$ , the total flux remained almost constant with height  
 437 (about  $5 \text{ ppb m s}^{-1}$ ) except a rapid increase near the ground level, which was ascribed to the  
 438 simulation approach here, in which the near-vehicle dispersion was assumed to exhibit a Gaussian  
 439 distribution. For  $\text{O}_x$ , the total flux increased with an increase in the vertical height up to about  $1.4$   
 440  $\text{ppb m s}^{-1}$  at the canyon roof level, which was about 2.8 times its raw emission flux (about  $0.5 \text{ ppb}$   
 441  $\text{m s}^{-1}$ ). This ratio was higher than that found by Bright et al. (2013) for the  $\text{AR}=1$  case (about 1.3  
 442 times). This was due to the  $\text{HO}_x$  chemistry, which converted  $\text{NO}$  to  $\text{NO}_2$  and thereby resulting in an  
 443 increase in  $\text{O}_x$ . Without the  $\text{HO}_x$  chemistry,  $\text{O}_x$  flux would be nearly constant in the canyon  
 444 environment because titration does not change the abundance of  $\text{O}_x$ . It was the longer retention  
 445 time of pollutants in the deep street canyon ( $\text{AR}=2$ ) that allowed the accumulation of  $\text{O}_x$  generated  
 446 from the  $\text{HO}_x$  chemistry. This was very different for the case with an  $\text{AR}=1$  (Bright et al., 2013)  
 447 with a much shorter retention time (residence time) for pollutants. The fluxes increased further with  
 448 the vertical height for the deep street canyon ( $\text{AR}=2$ ) in this study (with the canyon roof fluxes  
 449 around 2 times compared to those for the canyon with an  $\text{AR}=1$ ). These findings suggested that the  
 450 within-canyon pre-processing results in an increase in the oxidant flux and this effect is more  
 451 significant for the deeper street canyon.

### 452 4.3 Segregation effects

453 Table 1 lists intensities of segregation (in percentage) between selected pairs of chemical species for  
 454 the street canyon. It is interesting to note that  $I_{S(A+B)}$  for  $A=B$  are positive, with the largest value  
 455 of 28.49 % for  $I_{S(\text{NO}+\text{NO})}$ , and the smallest value of 0.36 % for  $I_{S(\text{OH}+\text{OH})}$ . This can be explained by  
 456 the fact that the auto-covariance of any chemical species was always positive if the chemical  
 457 species was not homogenously distributed within the canyon.  $I_{S(A+B)}$  (where  $A=B$ ) reflected the  
 458 spatial variability of the chemical species within the canyon relative to its mean concentration.

459 It was found that there were positive values for intensities of segregation between  $\text{NO}$ ,  $\text{NO}_2$  and  
 460 VOCs, indicating that ‘emitted chemical species’ have similar correlations and are driven by the

461 dynamical processes acting upon emissions. The highest value was found to be 22.32 % for  
462  $I_{S(NO+VOCs)}$ . These emitted chemical species were carried by the canyon vortices and removed from  
463 the canyon roof level to the background atmosphere. Positive values of intensities of segregation  
464 between  $O_3$ , OH and  $HO_2$  were also clearly observed, but these magnitudes were lower (below 3%) .  
465 This can be explained by considering that  $O_3$ , OH and  $HO_2$  are ‘entrained chemical species’ with  
466 higher levels in the background environment than those inside the street canyon and thereby  
467 exhibiting similar behaviour. This implied that segregation effect would enhance the rate of a  
468 reaction between pairs of species with similar origins.

469 It was also noted that negative values are found for intensities of segregation between emitted and  
470 entrained chemical species. This was attributed to the opposite origin of those chemical species.  
471 Negative correlations between those species were therefore expected. As shown in Table 1, these  
472 pairs of both emitted and entrained chemical species generally undergo the chemical reactions  
473 within the canyon. The average chemical reaction rates across the canyon domain were expected to  
474 be reduced due to the incomplete mixing in such an environment. Segregation effects were  
475 relatively larger between  $O_3$  and emitted species than those between OH (or  $HO_2$ ) and emitted  
476 species. It is noted that intensity of segregations are -11.09 % between NO and  $O_3$  (featured by  $O_3$   
477 titration) and -2.37 % between VOCs and OH (linked by fast radical reactions), which were about  
478 twice those calculated for a regular street canyon with an AR= 1 in Bright et al. (2013). It is not  
479 surprised that the segregation effect for a deep street canyon with two primary vortices is more  
480 significant than that for a regular street canyon with only one primary vortex (Bright et al., 2013).  
481 These findings showed that the NO and  $O_3$  titration to generate  $NO_2$  within the street canyon was  
482 reduced by 11.09 % and the conversion rate of NO to  $NO_2$  by the VOCs oxidation chemistry via  
483 the OH/ $HO_2$  chemistry was reduced by 2.37 % due to segregation effects, compared with a well-  
484 mixed system. In other words, if the whole street canyon was treated by a single well-mixed box,  
485 effective chemical reaction rates (Equation (25-27)) should be adopted, e.g. 11.09% smaller for NO  
486 and  $O_3$  and 2.37 % smaller for VOCs and OH, than the standard kinetic values for a well-mixed

487 system (or for the individual reactions in isolation). Such effective chemical reaction rates would  
 488 compensate for the immediate and total mixing assumption inherent in the single box approach - but  
 489 the change required would vary for each scenario (emissions, background chemistry, aspect ratio)  
 490 due to the non-linearity. Auger and Legras (2007) suggested that due to the nonlinear nature of  
 491 chemical processes, even a small value for intensity of segregation (e.g. 1 %) may lead to  
 492 substantial effects on the mean concentrations, especially where the pollutant residence time is short.

#### 493 **4.4 A coupled two-box model approximation**

494 Zhong et al. (2015) developed a simplified two-box model coupled with simple NO<sub>x</sub>-O<sub>3</sub> chemistry  
 495 to capture the concentration contrast between the lower canyon (box) and the upper canyon (box),  
 496 reflecting the potential segregation effect caused by the two counter-rotating vortices. By using a  
 497 plane at the level of  $z/H = \alpha$  (where  $\alpha$  is the box height ratio determined by the flow structure  
 498 with the street canyon; a value of 0.25 was approximated based on their LES results), the two-box  
 499 model framework for the deep street canyon was developed (Figure S2 in the Supplementary  
 500 Materials). The mathematical description of the two-box model is as follows:

$$501 \quad \frac{dC_{i,L}}{dt} = -\frac{w_{t,L}}{H_L}(C_{i,L} - C_{i,U}) + E_{i,L} + \Delta S_{i,L} \quad (28)$$

$$502 \quad \frac{dC_{i,U}}{dt} = \frac{w_{t,L}}{H_U}(C_{i,L} - C_{i,U}) - \frac{w_{t,U}}{H_U}(C_{i,U} - C_{i,b}) + \Delta S_{i,U} \quad (29)$$

503 where  $C_i$  (ppb) represents the concentration of  $i^{th}$  species;  $t$  (s) is the time;  $H$  (m) represents the  
 504 height;  $w_t$  (m s<sup>-1</sup>) represents the exchange velocity;  $E_i$  (ppb s<sup>-1</sup>) represent the emission rate of  $i^{th}$   
 505 species ;  $\Delta S_i$  represents the chemical source term of  $i^{th}$  species; “L” represent the properties for the  
 506 lower box while “U” represent the properties for the upper box. The exchange velocities employed  
 507 in the two-box model are 0.018 m s<sup>-1</sup> for  $w_{t,L}$  and 0.014 m s<sup>-1</sup> for  $w_{t,U}$ , which are derived based on  
 508 the LES model for the exchange of a passive scalar in Zhong et al. (2015). In this study, these

509 chemical sources terms in Equations (28) and (29) are derived from the RCS  $\text{O}_3$ - $\text{NO}_x$ -VOC  
510 chemistry rather than simple  $\text{NO}_x$ - $\text{O}_3$  chemistry in Zhong et al. (2015).

#### 511 4.4.1 Time evolution of volume-averaged concentrations

512 Figure 6 shows time evolution of volume-averaged concentrations of NO,  $\text{NO}_2$ ,  $\text{O}_3$ ,  $\text{NO}_x$ ,  $\text{O}_x$ , OH  
513 and  $\text{HO}_2$  for the lower and upper canyon (box) calculated by the LES-chemistry model and the two-  
514 box model, respectively. In Figure 6, it is interesting that there were fluctuations for the LES  
515 approach due to its inherently unsteady (dynamical) nature. It was observed that there were rapid  
516 changes in mixing ratios when the emissions were released into the street canyon from 30 min.  
517 Compared with the LES-chemistry model over the period of 180-240 min (volume- and time-  
518 averaged mixing ratios listed in Table 2), the two-box model underestimated NO levels by about  
519 5.25 % and 5.8 % for, but overestimated  $\text{NO}_2$  levels by about 8.47 % and 5.94 % for the lower and  
520 upper boxes respectively. Levels of  $\text{O}_3$  derived from the two-box model were about 1.97 % and  
521 1.83 % lower than those derived from the LES-chemistry model for the lower and upper boxes  
522 respectively. These differences were small, suggesting that the two-box approach performs pretty  
523 well compared with the “more realistic” LES-chemistry model. These results also showed that  
524 segregation effects caused by incomplete mixing (i.e. spatial inhomogeneity represented by the  
525 LES-chemistry model) reduced the conversion rate of NO to  $\text{NO}_2$  through chemistry (dominated by  
526 NO and  $\text{O}_3$  titration with an additional pathway through VOCs chemistry), which was consistent  
527 with negative values of intensities of segregation between NO and  $\text{O}_3$ , and between OH and VOCs  
528 (Table 1). It was also observed that  $\text{NO}_2/\text{NO}$  ratios in the two-box model were generally higher than  
529 those in the LES-chemistry model, i.e. about 14.47 % for the lower box and about 12.50 % for the  
530 upper box. Therefore, there were higher levels of  $\text{O}_3$  and NO, but lower levels of  $\text{NO}_2$  in the LES-  
531 chemistry model than those in the two-box model for both lower and upper boxes. The LES-  
532 chemistry model had slightly higher levels of  $\text{NO}_x$  (about 1.59 % for the lower box and 1.69 % for  
533 the upper box) compared with the two-box model, which suggests that segregation effects slightly  
534 reduced the  $\text{NO}_x$  loss rate to other species (e.g.  $\text{HNO}_3$  and HONO). This was also consistent with



negative values of intensities of segregation between OH and NO<sub>2</sub>, and between OH and NO (Table 1). Lower levels of O<sub>x</sub> were observed in the LES-chemistry model compared with the two-box model, i.e. about 7.89 % for the lower box and 5.15 % for the upper box. This indicated that segregation effects generally reduced the rate of oxidation chemistry for both the lower and upper boxes. It was also observed that the two-box model slightly underestimated levels of both OH and HO<sub>2</sub> (generally around 1%) compared with the LES-chemistry model. This may be explained as levels of OH and HO<sub>2</sub> were low within street canyons and their reactions with other chemical species were very fast. Segregation effects can reduce the rate for some of these chemical reactions, but increased the rate for other chemical reactions (Table 1). The total segregation effect may be somewhat balanced out - depending upon the metric under consideration, i.e. which species is concerned. In terms of overall performance, the two-box model generally matched the LES approach in the volume averaged concentrations of pollutants for both the lower and upper boxes.

## 5 Conclusions

An LES model coupled with O<sub>3</sub>-NO<sub>x</sub>-VOC chemistry (the RCS mechanism) was implemented to simulate the coupling effect of emissions, mixing and chemical pre-processing within a deep urban street canyon (AR=2). There were significant spatial variations of reactive pollutants in the presence of two vertically aligned unsteady vortices formed in the canyon. Compared with the RCS mechanism, simple NO<sub>x</sub>-O<sub>3</sub> chemistry overestimated NO level, but underestimated levels of NO<sub>2</sub> and O<sub>3</sub>, indicating the additional conversion of NO to NO<sub>2</sub> through OH/HO<sub>2</sub> chemistry. NO, NO<sub>x</sub>, O<sub>3</sub>, OH and HO<sub>2</sub> were chemically consumed, while NO<sub>2</sub> and O<sub>x</sub> (oxidants) were chemically produced within the canyon environment. The within-canyon pre-processing would lead to chemical conversion of NO to NO<sub>2</sub> and an increase in the oxidant fluxes released from the canyon to the overlying canopy layer, and this effect was more significant for the deeper street canyon than the regular canyon (AR=1) (Bright et al., 2013). Consequently, urban canopy layer air quality in cities will vary systematically with the street architecture (aspect ratio), with greater release of NO<sub>2</sub>

560 and  $O_x$ , for the same traffic emissions, where street canyons are taller - for example in many  
561 traditional European city centres, in contrast to more open suburban regions. Such findings can be  
562 of importance in guiding the development of atmospheric pollutant flux parameterisation schemes  
563 for larger scale (e.g. city or regional scale) models, and for urban planning considerations. There  
564 was clear evidence of two distinctive behaviours for emitted chemical species and entrained  
565 chemical species. Positive (or negative) values of intensities of segregation were found between  
566 pairs of species with a similar (or opposite) behaviour. Such findings indicated that segregation  
567 effects were of importance in the incomplete mixing environment (e.g. the street canyon) with  
568 chemical processing involved. The simplified two-box model underestimated  $NO$  and  $O_3$  levels, but  
569 overestimated  $NO_2$  levels for both the lower and upper boxes compared with the LES-chemistry  
570 model.  $NO_2/NO$  ratios in the two-box model were found to be much higher than those in the LES-  
571 chemistry model. Segregation effects due to incomplete mixing may reduce the conversion rate of  
572  $NO$  to  $NO_2$  through chemistry.

## 573 **6 Implications and future research**

574 The LES-chemistry model in this study reveals the impacts of nonlinear  $O_3$ - $NO_x$ -VOC  
575 photochemical processes in the incomplete mixing environment (e.g. street canyons) and provides a  
576 better understanding of the pre-processing of emissions in the presence of both the street canyon  
577 dynamics and chemistry. This research may guide the location of new urban air quality stations, to  
578 ensure these are representative of human exposure and/or understand the measurement bias that  
579 may accrue from a particular location within a canyon. Because of the high computational cost, this  
580 study was limited to one typical emission scenario, with relatively poor air ventilation under neutral  
581 conditions. Also, due to the simple assumption of the idealised street canyon geometry under  
582 perpendicular ambient wind, flow field within the canyon was dominated by flow recirculation (i.e.  
583 two vortices). However, the current LES model of idealised scenarios does not capture lateral  
584 channelling flow (e.g. Longley et al., 2004) or even helical flow (e.g. Dobre et al., 2005; Barlow et

585 al., 2009) present in real, complex urban street canyons (Smalley et al., 2008). Future studies may  
586 consider the effects of other factors, such as complex urban configurations, wind speed, oblique  
587 wind directions, emissions and thermal/shading effects (e.g. Li et al., 2015; Li et al., 2016; Cheng  
588 and Liu, 2011b), on both the dynamic and chemical processing of reactive pollutants.

## 589 **Acknowledgements**

590 The computations described herein were performed using the University of Birmingham's  
591 BlueBEAR HPC service (<http://www.bear.bham.ac.uk>). The authors would like to thank Dr Vivien  
592 Bright for provision of the reduced chemical scheme (RCS). JZ thanks to the University of  
593 Birmingham for the award of a Li Siguang Scholarship, offered in partnership with the China  
594 Scholarship Council (CSC).

595

596

597

598

599

600

601

602

603

604

605

606 **Table 1 Intensities of segregation (in percentage) between pairs of chemical species for the street canyon. Values**  
 607 **shown in parentheses and bold denote those pairs of chemical species that react directly with each other in the**  
 608 **RCS O<sub>3</sub>-NO<sub>x</sub>-VOC chemistry. Positive (negative) values mean that these pairs of chemical species have similar**  
 609 **(opposite) behaviours.**

	O <sub>3</sub>	NO	NO <sub>2</sub>	VOCs	HO <sub>2</sub>	OH
O <sub>3</sub>	6.34	–	–	–	–	–
NO	<b>(-11.09)</b>	<b>(28.49)</b>	–	–	–	–
NO <sub>2</sub>	<b>(-5.10)</b>	11.18	4.73	–	–	–
VOCs	<b>(-8.91)</b>	22.32	8.86	17.51	–	–
HO <sub>2</sub>	<b>(2.87)</b>	<b>(-5.67)</b>	<b>(-2.44)</b>	<b>(-4.51)</b>	<b>(1.39)</b>	–
OH	<b>(1.25)</b>	<b>(-3.03)</b>	<b>(-1.17)</b>	<b>(-2.37)</b>	<b>(0.66)</b>	0.36

610

611

612 **Table 2 Volume- and time-averaged (over the period of 180-240 min) mixing ratios in the lower and upper boxes**  
 613 **derived from the LES-chemistry model (LES-RCS) and the two-box model (BOX-RCS), respectively. Positive**  
 614 **(negative) values represent the amount of overestimation (underestimation) by BOX-RCS compared with LES-**  
 615 **RCS.**

	Mixing ratio (ppb) for Lower Box			Mixing ratio (ppb) for Upper Box		
	(A) LES-RCS	(B) Box-RCS	[(B)-(A)]/(A) %	(C) LES-RCS	(D) Box-RCS	[(D)-(C)]/(C) %
180-237m						
O <sub>3</sub>	9.7858	9.59	-1.9722	14.25	13.9900	-1.8367
NO	462.4665	438.18	-5.2507	231.31	217.8370	-5.8252
NO <sub>2</sub>	168.1708	182.41	8.4653	125.36	132.8130	5.9425
OH(pppt)	0.103619	0.1023	-1.2482	0.1115	0.1111	-0.4080
HO <sub>2</sub> (pppt)	0.265364	0.2640	-0.4991	0.3210	0.3186	-0.7387
NO <sub>x</sub>	630.6373	620.5910	-1.5930	356.6747	350.6500	-1.6891
O <sub>x</sub>	177.9566	191.9999	7.8914	139.6151	146.8030	5.1484
HO <sub>x</sub>	0.3690	0.3664	-0.7095	0.4325	0.4297	-0.6534
NO <sub>2</sub> /NO	0.3636	0.4163	14.4761	0.5420	0.6097	12.4956

616

617

618

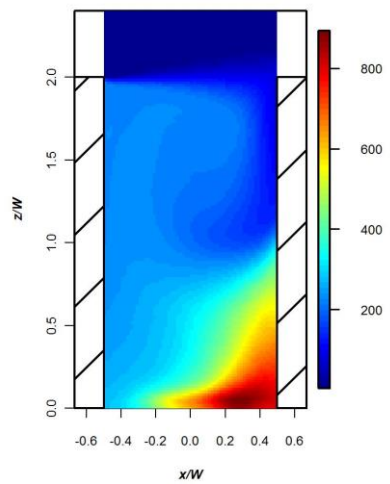
619

620

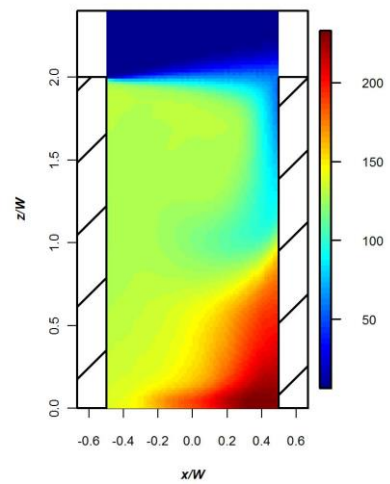
621

622

(a) NO



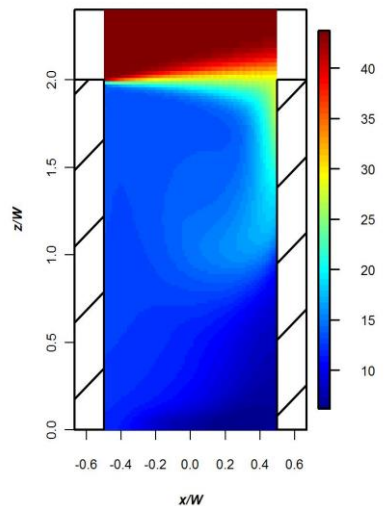
(b) NO<sub>2</sub>



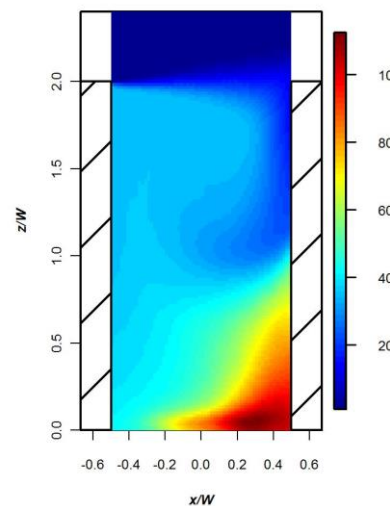
623

624

(c) O<sub>3</sub>



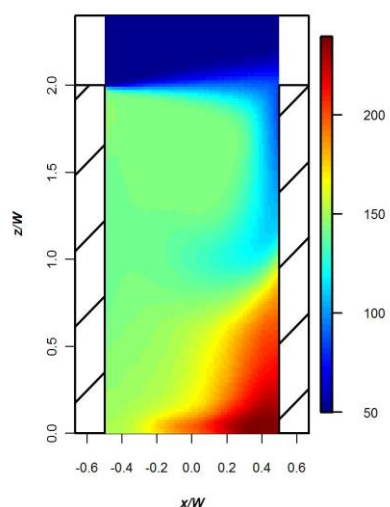
(d) NO<sub>x</sub>



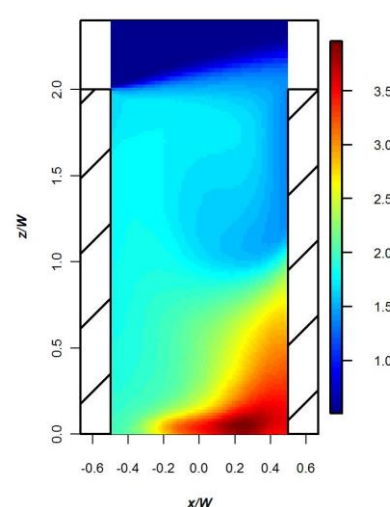
625

626

(e) O<sub>x</sub>



(f) NO/NO<sub>2</sub>



627

628

(g) OH



(h) HO<sub>2</sub>



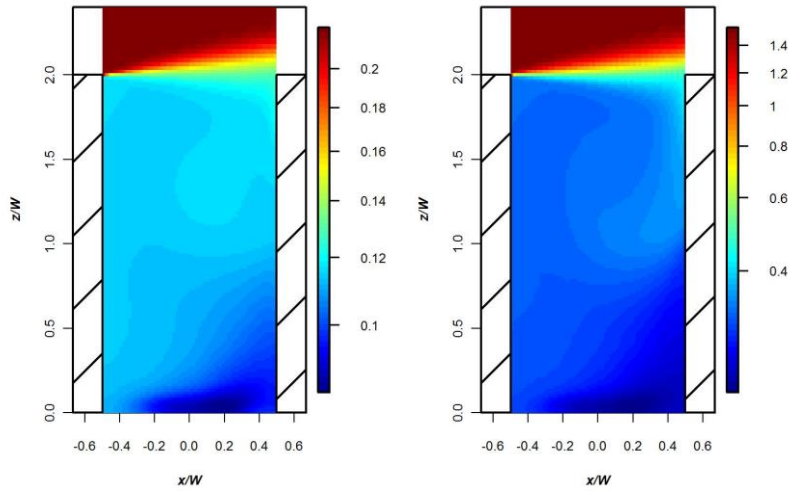
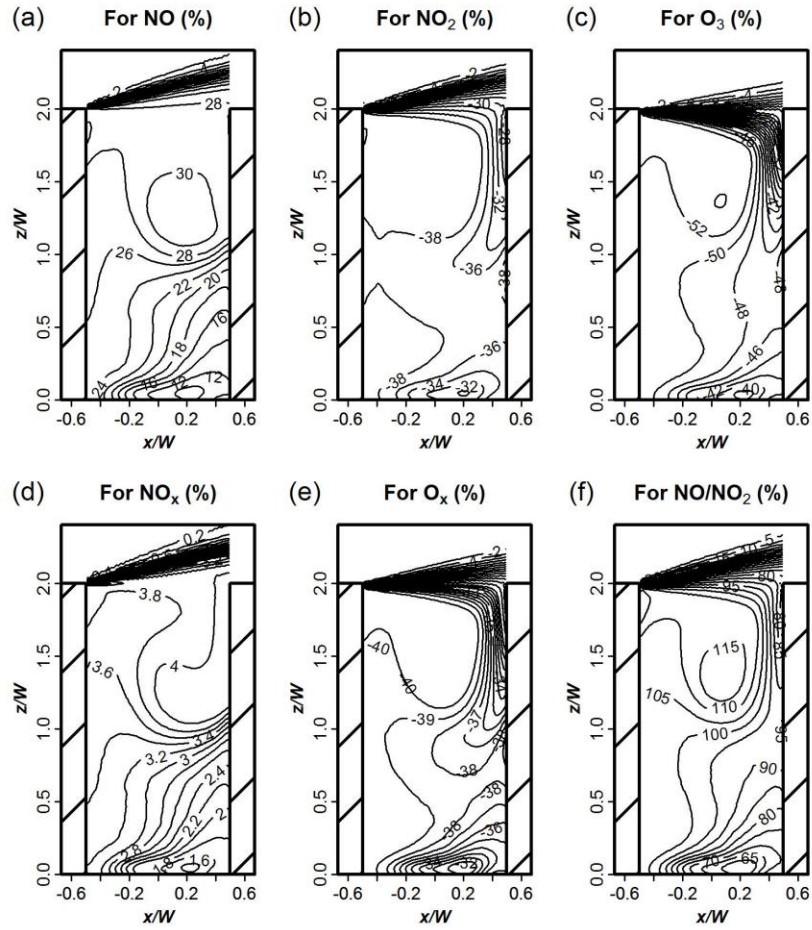


**Figure 1 Spatial variation of (a)  $\langle \overline{NO} \rangle$  (ppb), (b)  $\langle \overline{NO_2} \rangle$  (ppb), (c)  $\langle \overline{O_3} \rangle$  (ppb), (d)  $\langle \overline{NO_x} \rangle$  (ppb), (e)  $\langle \overline{O_x} \rangle$  (ppb), and (f)  $\langle \overline{NO} \rangle / \langle \overline{NO_2} \rangle$ , (g)  $\langle \overline{OH} \rangle$  (ppt) and (h)  $\langle \overline{HO_2} \rangle$  (ppt). Logarithmic colour scales are applied for  $\langle \overline{OH} \rangle$  and  $\langle \overline{HO_2} \rangle$ .**



654

655

656

657

658

659

Figure 2 Spatial variations of the overestimation of the spatially and temporally averaged concentrations (%) by simple NO<sub>x</sub>-O<sub>3</sub> chemistry compared with the RCS chemical mechanism for (a)  $\langle \overline{NO} \rangle$ , (b)  $\langle \overline{NO_2} \rangle$ , (c)  $\langle \overline{O_3} \rangle$ , (d)  $\langle \overline{NO_x} \rangle$ , (e)  $\langle \overline{O_x} \rangle$  and (f)  $\langle \overline{NO} \rangle / \langle \overline{NO_2} \rangle$ .

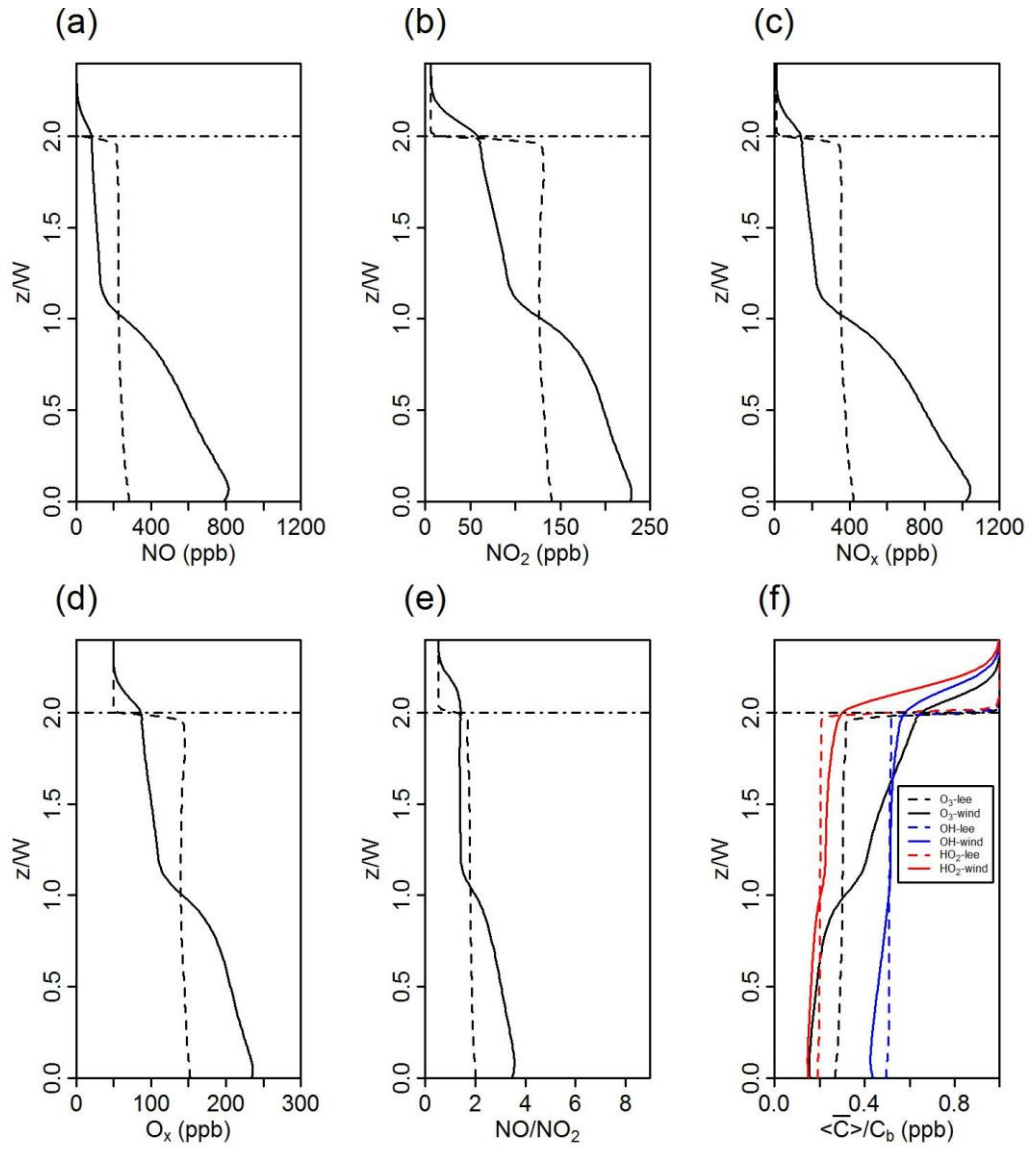
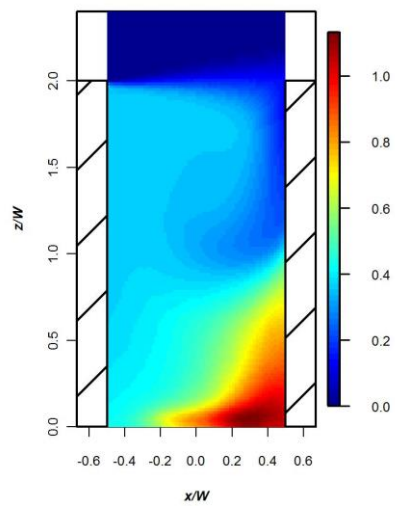


**Figure 3** Vertical profiles of (a)  $\langle \overline{NO} \rangle$ , (b)  $\langle \overline{NO_2} \rangle$ , (c)  $\langle \overline{NO_x} \rangle$ , (d)  $\langle \overline{O_3} \rangle$ , (e)  $\langle \overline{NO} \rangle / \langle \overline{NO_2} \rangle$ , and (f)  $\langle \overline{C} \rangle / C_b$  (for  $O_3$ ,  $OH$  and  $HO_2$  normalised by their background levels) along the leeward and windward walls, represented by the dash and solid lines respectively.

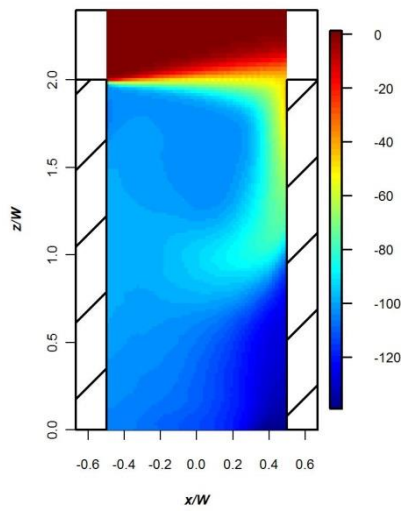


670

(a)  $C_{emn,1}$



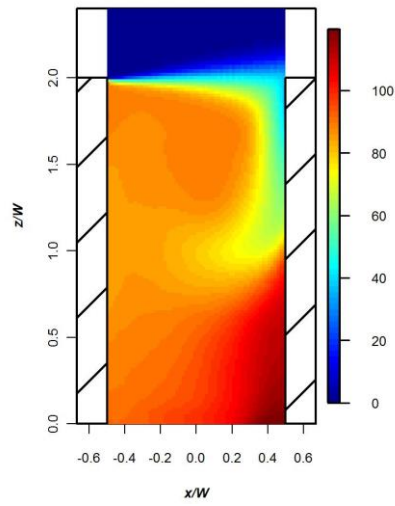
(b)  $C_{chem}$  for NO



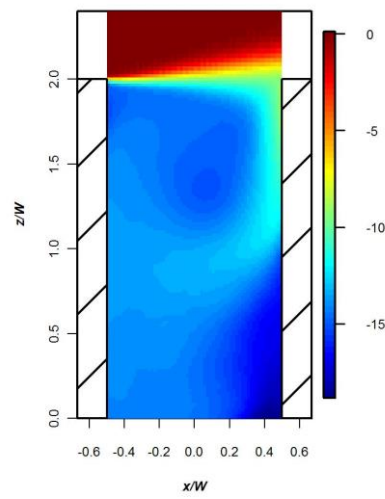
671

672

(c)  $C_{chem}$  for NO<sub>2</sub>



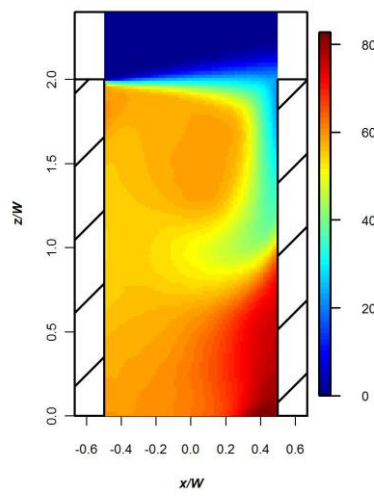
(d)  $C_{chem}$  for NO<sub>x</sub>



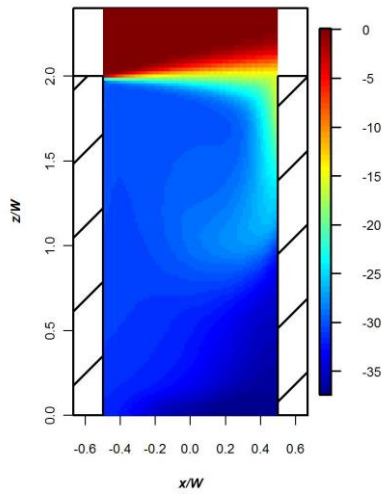
673

674

(e)  $C_{chem}$  for O<sub>x</sub>



(f)  $C_{chem}$  for O<sub>3</sub>



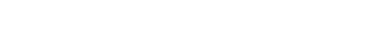
675

676

(g)  $C_{chem}$  for OH



(h)  $C_{chem}$  for HO<sub>2</sub>



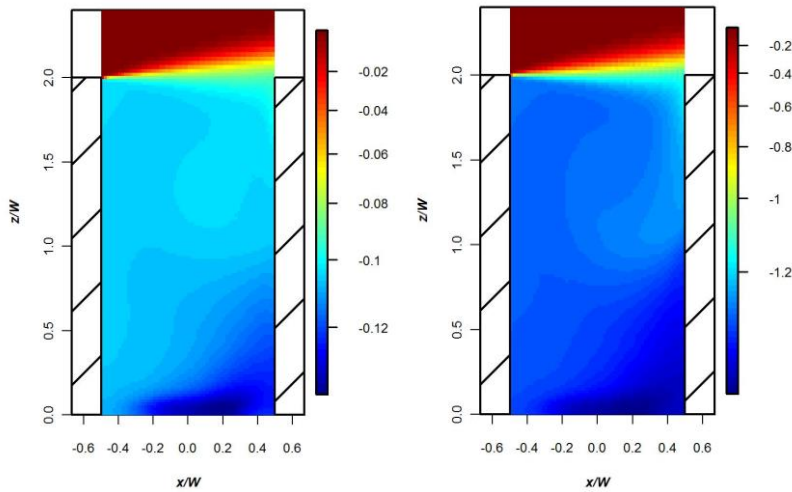


Figure 4 Spatial variation of (a)  $C_{emn,1}$  (ppb) and  $C_{chem}$  of (b) NO (ppb), (c) NO<sub>2</sub> (ppb), (d) NO<sub>x</sub> (ppb), (e) O<sub>x</sub> (ppb), (f) O<sub>3</sub> (ppb), (g) OH (ppt) and (h) HO<sub>2</sub> (ppt). Logarithmic colour scales are applied for OH and HO<sub>2</sub>. Note very different colour scales for different species.

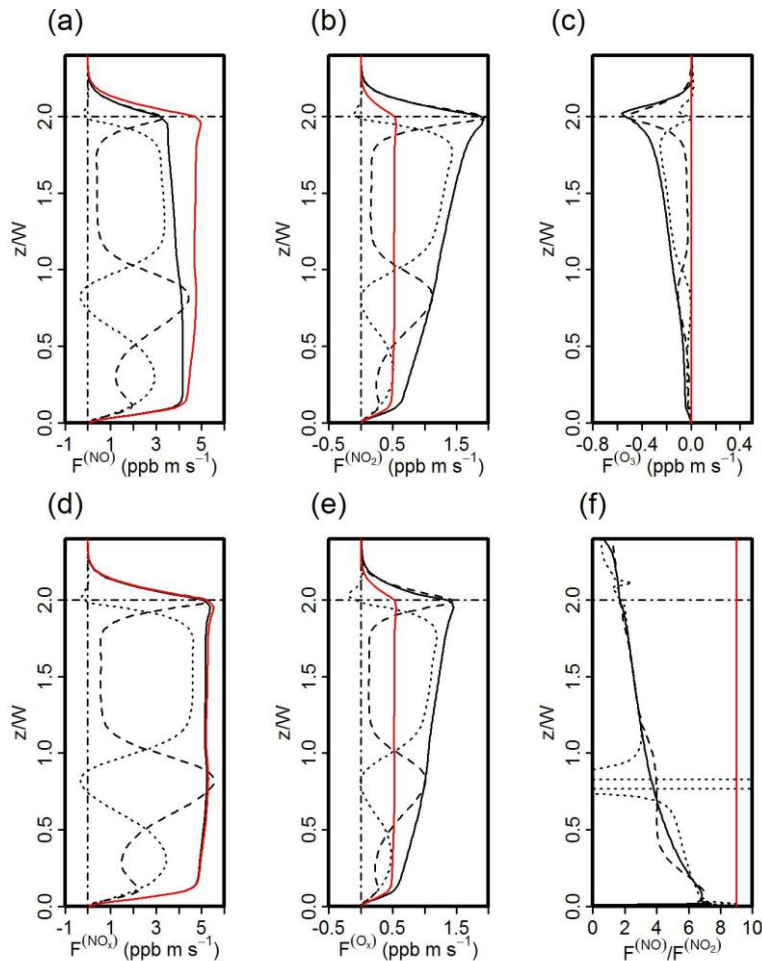
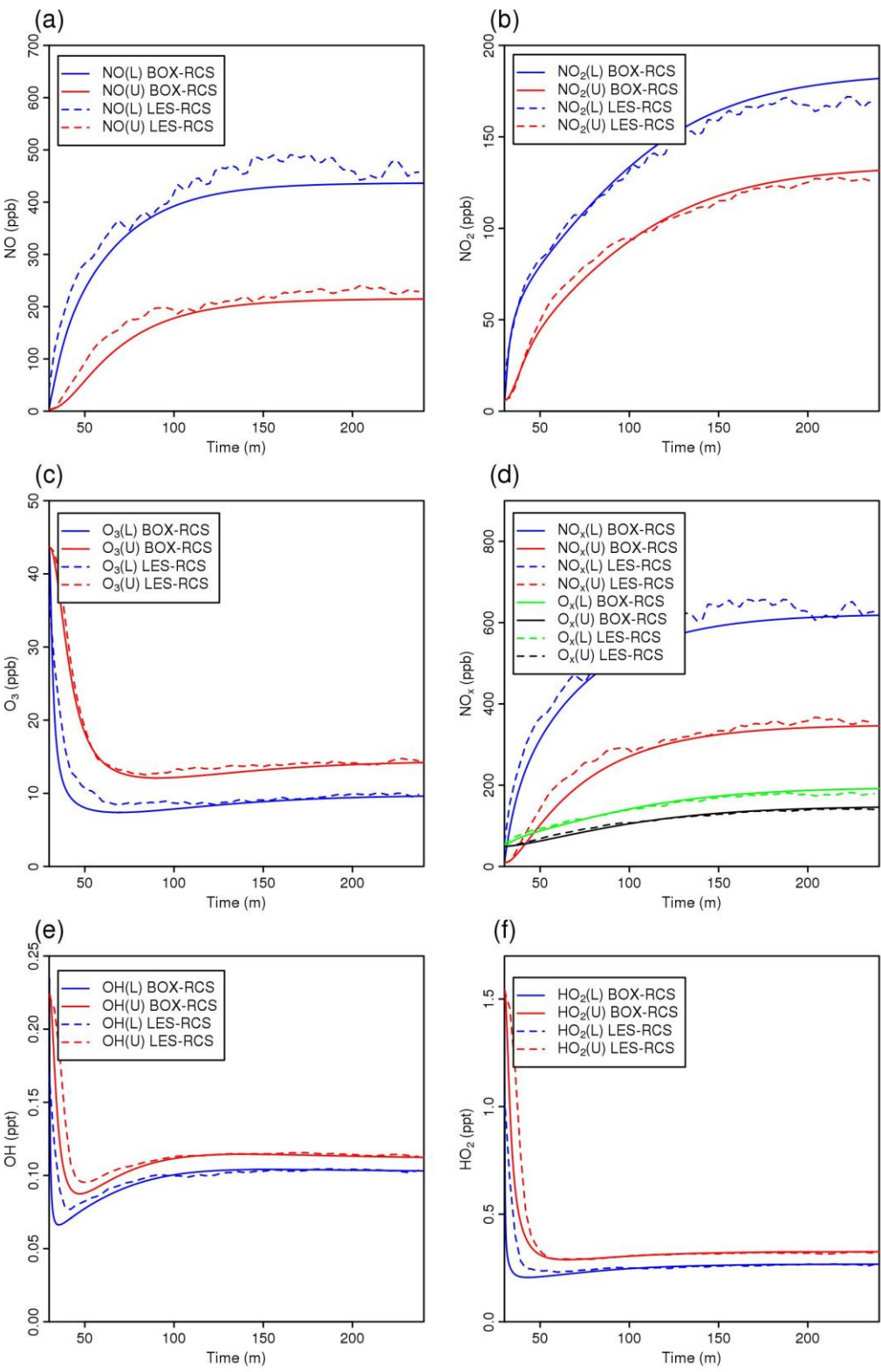


Figure 5 Vertical profiles of the horizontally averaged total, turbulent and advective fluxes for (a) NO, (b) NO<sub>2</sub>, (c) O<sub>3</sub>, (d) NO<sub>x</sub>, (e) O<sub>x</sub> and (f) NO/NO<sub>2</sub>. The total, turbulent and advective fluxes for each quantity are represented by the black solid, dash and dotted lines, respectively. The total fluxes for non-passive scalars assuming no chemical reactions (i.e. reconstructed based on a passive scalar with a unit emission rate) are denoted by red solid lines.



690 **Figure 6** Time evolution of the volume averaged concentrations of (a) NO, (b) NO<sub>2</sub>, (c) O<sub>3</sub>, (d) NO<sub>x</sub> and O<sub>x</sub>, (e)  
691 OH and (f) HO<sub>2</sub> derived from the LES-chemistry model (LES-RCS) and the two-box model (BOX-RCS),  
692 respectively. ‘L’ represents the lower box while ‘U’ represents the upper box.

695 **References:**

- 696 AHMAD, K., KHARE, M. & CHAUDHRY, K. K. 2005. Wind tunnel simulation studies on  
697 dispersion at urban street canyons and intersections - a review. *Journal of Wind Engineering*  
698 *and Industrial Aerodynamics*, 93, 697-717.
- 699 ALEXANDROV, A., SAMEH, A., SIDDIQUE, Y. & ZLATEV, Z. 1997. Numerical integration of  
700 chemical ODE problems arising in air pollution models. *Environmental Modeling &*  
701 *Assessment*, 2, 365-377.
- 702 AUGER, L. & LEGRAS, B. 2007. Chemical segregation by heterogeneous emissions. *Atmospheric*  
703 *Environment*, 41, 2303-2318.
- 704 BAKER, J., WALKER, H. L. & CAI, X. M. 2004. A study of the dispersion and transport of  
705 reactive pollutants in and above street canyons - a large eddy simulation. *Atmospheric*  
706 *Environment*, 38, 6883-6892.
- 707 BARLOW, J. F., DOBRE, A., SMALLEY, R. J., ARNOLD, S. J., TOMLIN, A. S. & BELCHER, S.  
708 E. 2009. Referencing of street-level flows measured during the DAPPLE 2004 campaign.  
709 *Atmospheric Environment*, 43, 5536-5544.
- 710 BLOSS, C., WAGNER, V., JENKIN, M. E., VOLKAMER, R., BLOSS, W. J., LEE, J. D., HEARD,  
711 D. E., WIRTZ, K., MARTIN-REVIEJO, M., REA, G., WENGER, J. C. & PILLING, M. J.  
712 2005. Development of a detailed chemical mechanism (MCMv3.1) for the atmospheric  
713 oxidation of aromatic hydrocarbons. *Atmospheric Chemistry and Physics*, 5, 641-664.
- 714 BLOSS, W. J. 2009. Atmospheric Chemical Processes of Importance in Cities. In: *Harrison, R. M.*  
715 *& Hester, R. E. (eds.) Air Quality in Urban Environments*, Cambridge: The Royal Society of  
716 Chemistry.
- 717 BOULTER, P. G., BARLOW, T. J., S., L. & S., M. I. 2009. Emission factors 2009: Report 1-a  
718 review of methods for determining hot exhaust emission factors for road vehicles.  
719 *TRL: Wokingham, UK*.
- 720 BRIGHT, V. B. 2013. *Street canyon atmospheric composition: coupling dynamics and chemistry*.  
721 Ph.D. thesis, University of Birmingham.
- 722 BRIGHT, V. B., BLOSS, W. J. & CAI, X. M. 2013. Urban street canyons: Coupling dynamics,  
723 chemistry and within-canyon chemical processing of emissions. *Atmospheric Environment*,  
724 68, 127-142.
- 725 CHENG, W. C. & LIU, C.-H. 2011a. Large-Eddy Simulation of Flow and Pollutant Transports in  
726 and Above Two-Dimensional Idealized Street Canyons. *Boundary-Layer Meteorology*, 139,  
727 411-437.
- 728 CHENG, W. C. & LIU, C. H. 2011b. Large-eddy simulation of turbulent transports in urban street  
729 canyons in different thermal stabilities. *Journal of Wind Engineering and Industrial*  
730 *Aerodynamics*, 99, 434-442.
- 731 DEFRA 2008. The Air Quality Strategy for England, Scotland, Wales and Northern Ireland.  
732 Volume 1.
- 733 DOBRE, A., ARNOLD, S. J., SMALLEY, R. J., BODDY, J. W. D., BARLOW, J. F., TOMLIN, A.  
734 S. & BELCHER, S. E. 2005. Flow field measurements in the proximity of an urban  
735 intersection in London, UK. *Atmospheric Environment*, 39, 4647-4657.
- 736 DUNMORE, R. E., HOPKINS, J. R., LIDSTER, R. T., LEE, J. D., EVANS, M. J., RICKARD, A.  
737 R., LEWIS, A. C. & HAMILTON, J. F. 2015. Diesel-related hydrocarbons can dominate  
738 gas phase reactive carbon in megacities. *Atmospheric Chemistry and Physics*, 15, 9983-9996.
- 739 HEARD, D. E. & PILLING, M. J. 2003. Measurement of OH and HO<sub>2</sub> in the troposphere.  
740 *Chemical Reviews*, 103, 5163-5198.
- 741 HERTEL, O., BERKOWICZ, R., CHRISTENSEN, J. & HOV, O. 1993. TEST OF 2 NUMERICAL  
742 SCHEMES FOR USE IN ATMOSPHERIC TRANSPORT-CHEMISTRY MODELS.  
743 *Atmospheric Environment Part a-General Topics*, 27, 2591-2611.
- 744 HESSTVEDT, E., HOV, O. & ISAKSEN, I. S. A. 1978. QUASI-STEADY-STATE  
745 APPROXIMATIONS IN AIR-POLLUTION MODELING - COMPARISON OF TWO

746 NUMERICAL SCHEMES FOR OXIDANT PREDICTION. *International Journal of*  
747 *Chemical Kinetics*, 10, 971-994.

748 HILST, G. R. 1998. Segregation and chemical reaction rates in air quality models. *Atmospheric*  
749 *Environment*, 32, 3891-3895.

750 JACOBSON, M. Z. 2005. *Fundamentals of Atmospheric Modeling*, New York, Cambridge  
751 University Press.

752 JENKIN, M. E., SAUNDERS, S. M., DERWENT, R. G. & PILLING, M. J. 1997. Construction and  
753 application of a master chemical mechanism (MCM) for modelling tropospheric chemistry.  
754 *Abstracts of Papers of the American Chemical Society*, 214, 116-COLL.

755 JENKIN, M. E., SAUNDERS, S. M., WAGNER, V. & PILLING, M. J. 2003. Protocol for the  
756 development of the Master Chemical Mechanism, MCM v3 (Part B): tropospheric  
757 degradation of aromatic volatile organic compounds. *Atmospheric Chemistry and Physics*, 3,  
758 181-193.

759 JENKIN, M. E., WATSON, L. A., UTEMBE, S. R. & SHALLCROSS, D. E. 2008. A Common  
760 Representative Intermediates (CRI) mechanism for VOC degradation. Part 1: Gas phase  
761 mechanism development. *Atmospheric Environment*, 42, 7185-7195.

762 KROL, M. C., MOLEMAKER, M. J. & DE ARELLANO, J. V. G. 2000. Effects of turbulence and  
763 heterogeneous emissions on photochemically active species in the convective boundary  
764 layer. *Journal of Geophysical Research-Atmospheres*, 105, 6871-6884.

765 KWAK, K. H. & BAIK, J. J. 2012. A CFD modeling study of the impacts of NO<sub>x</sub> and VOC  
766 emissions on reactive pollutant dispersion in and above a street canyon. *Atmospheric*  
767 *Environment*, 46, 71-80.

768 KWAK, K. H., BAIK, J. J. & LEE, K. Y. 2013. Dispersion and photochemical evolution of reactive  
769 pollutants in street canyons. *Atmospheric Environment*, 70, 98-107.

770 LI, X.-X., LEUNG, D. Y. C., LIU, C.-H. & LAM, K. M. 2008a. Physical modeling of flow field  
771 inside urban street canyons. *Journal of Applied Meteorology and Climatology*, 47, 2058-  
772 2067.

773 LI, X.-X., LIU, C.-H. & LEUNG, D. Y. C. 2008b. Large-eddy simulation of flow and pollutant  
774 dispersion in high-aspect-ratio urban street canyons with wall model. *Boundary-Layer*  
775 *Meteorology*, 129, 249-268.

776 LI, X. X., BRITTER, R. & NORFORD, L. K. 2016. Effect of stable stratification on dispersion  
777 within urban street canyons: A large-eddy simulation. *Atmospheric Environment*, 144, 47-59.

778 LI, X. X., BRITTER, R. E. & NORFORD, L. K. 2015. Transport processes in and above two-  
779 dimensional urban street canyons under different stratification conditions: results from  
780 numerical simulation. *Environmental Fluid Mechanics*, 15, 399-417.

781 LI, X. X., BRITTER, R. E., NORFORD, L. K., KOH, T. Y. & ENTEKHABI, D. 2012. Flow and  
782 Pollutant Transport in Urban Street Canyons of Different Aspect Ratios with Ground  
783 Heating: Large-Eddy Simulation. *Boundary-Layer Meteorology*, 142, 289-304.

784 LI, X. X., LIU, C. H., LEUNG, D. Y. C. & LAM, K. M. 2006. Recent progress in CFD modelling  
785 of wind field and pollutant transport in street canyons. *Atmospheric Environment*, 40, 5640-  
786 5658.

787 LIU, C. H., LEUNG, D. Y. C. & BARTH, M. C. 2005. On the prediction of air and pollutant  
788 exchange rates in street canyons of different aspect ratios using large-eddy simulation.  
789 *Atmospheric Environment*, 39, 1567-1574.

790 LONGLEY, I. D., GALLAGHER, M. W., DORSEY, J. R., FLYNN, M. & BARLOW, J. F. 2004.  
791 Short-term measurements of airflow and turbulence in two street canyons in Manchester.  
792 *Atmospheric Environment*, 38, 69-79.

793 MAYER, H. 1999. Air pollution in cities. *Atmospheric Environment*, 33, 4029-4037.

794 MURENA, F., FAVALE, G., VARDOULAKIS, S. & SOLAZZO, E. 2009. Modelling dispersion of  
795 traffic pollution in a deep street canyon: Application of CFD and operational models.  
796 *Atmospheric Environment*, 43, 2303-2311.

- NEOPHYTOU, M. K., GOUSSIS, D. A., VAN LOON, M. & MASTORAKOS, E. 2004. Reduced chemical mechanisms for atmospheric pollution using Computational Singular Perturbation analysis. *Atmospheric Environment*, 38, 3661-3673.
- OPENFOAM 2012. <http://www.openfoam.com/>. Accessed May 2012.
- PINHO, P. G., PIO, C. A., CARTER, W. P. L. & JENKIN, M. E. 2007. Evaluation of alpha- and beta-pinene degradation in the detailed tropospheric chemistry mechanism, MCM v3.1, using environmental chamber data. *Journal of Atmospheric Chemistry*, 57, 171-202.
- SALIM, S. M., BUCCOLIERI, R., CHAN, A. & DI SABATINO, S. 2011. Numerical simulation of atmospheric pollutant dispersion in an urban street canyon: Comparison between RANS and LES. *Journal of Wind Engineering and Industrial Aerodynamics*, 99, 103-113.
- SALIZZONI, P., SOULHAC, L. & MEJEAN, P. 2009. Street canyon ventilation and atmospheric turbulence. *Atmospheric Environment*, 43, 5056-5067.
- SAUNDERS, S. M., JENKIN, M. E., DERWENT, R. G. & PILLING, M. J. 2003. Protocol for the development of the Master Chemical Mechanism, MCM v3 (Part A): tropospheric degradation of non-aromatic volatile organic compounds. *Atmospheric Chemistry and Physics*, 3, 161-180.
- SCHLICHTING, H. & GERSTEN, K. 2000. Boundary layer theory. *Springer*, Berlin.
- SMALLEY, R. J., TOMLIN, A. S., DIXON, N. S. & BODDY, J. W. D. 2008. The influence of background wind direction on the roadside turbulent velocity field within a complex urban street. *Quarterly Journal of the Royal Meteorological Society*, 134, 1371-1384.
- VARDOULAKIS, S., FISHER, B. E. A., PERICLEOUS, K. & GONZALEZ-FLESCA, N. 2003. Modelling air quality in street canyons: a review. *Atmospheric Environment*, 37, 155-182.
- VERWER, J. G. & SIMPSON, D. 1995. EXPLICIT METHODS FOR STIFF ODES FROM ATMOSPHERIC CHEMISTRY. *Applied Numerical Mathematics*, 18, 413-430.
- VERWER, J. G. & VAN LOON, M. 1994. AN EVALUATION OF EXPLICIT PSEUDO-STEADY-STATE APPROXIMATION SCHEMES FOR STIFF ODE SYSTEMS FROM CHEMICAL-KINETICS. *Journal of Computational Physics*, 113, 347-352.
- VINUESA, J. F. & DE ARELLANO, J. V. G. 2005. Introducing effective reaction rates to account for the inefficient mixing of the convective boundary layer. *Atmospheric Environment*, 39, 445-461.
- YAZID, A. W. M., SIDIK, N. A. C., SALIM, S. M. & SAQR, K. M. 2014. A review on the flow structure and pollutant dispersion in urban street canyons for urban planning strategies. *Simulation-Transactions of the Society for Modeling and Simulation International*, 90, 892-916.
- ZHONG, J., CAI, X. & BLOSS, W. J. 2014. Modelling segregation effects of heterogeneous emissions on ozone levels in idealised urban street canyons: Using photochemical box models *Environmental Pollution*, 188, 132-143.
- ZHONG, J., CAI, X. & BLOSS, W. J. 2015. Modelling the dispersion and transport of reactive pollutants in a deep urban street canyon: Using large-eddy simulation. *Environmental Pollution*, 200, 42-52.
- ZHONG, J., CAI, X. & BLOSS, W. J. 2016. Coupling dynamics and chemistry in the air pollution modelling of street canyons: A review. *Environmental Pollution*, 214, 690-704.